Apical Ca^{2+}-activated potassium channels in mouse parotid acinar cells

Janos Almassy, Jong Hak Won, Ted B. Begenisich, and David I. Yule

Department of Pharmacology and Physiology, University of Rochester Medical Center, University of Rochester, Rochester, NY 14642

Ca^{2+} activation of Cl and K channels is a key event underlying stimulated fluid secretion from parotid salivary glands. Cl channels are exclusively present on the apical plasma membrane (PM), whereas the localization of K channels has not been established. Mathematical models have suggested that localization of some K channels to the apical PM is optimum for fluid secretion. A combination of whole cell electrophysiology and temporally resolved digital imaging with local manipulation of intracellular [Ca^{2+}] was used to investigate if Ca^{2+}-activated K channels are present in the apical PM of parotid acinar cells. Initial experiments established Ca^{2+}-buffering conditions that produced brief, localized increases in [Ca^{2+}] after focal laser photolysis of caged Ca^{2+}. Conditions were used to isolate K^+ and Cl^- conductances. Photolysis at the apical PM resulted in a robust increase in K^+ and Cl^- currents. A localized reduction in [Ca^{2+}] at the apical PM after photolysis of Diazo-2, a caged Ca^{2+} chelator, resulted in a decrease in both K^+ and Cl^- currents. The K^+ currents evoked by apical photolysis were partially blocked by both paxilline and TRAM-34, specific blockers of large-conductance "maxi-K" (BK) and intermediate K (IK), respectively, and almost abolished by incubation with both antagonists. Apical TRAM-34–sensitive K^+ currents were also observed in BK-null parotid acini. In contrast, when the [Ca^{2+}] was increased at the basal or lateral PM, no increase in either K^+ or Cl^- currents was evoked. These data provide strong evidence that K and Cl channels are similarly distributed in the apical PM. Furthermore, both IK and BK channels are present in this domain, and the density of these channels appears higher in the apical versus basolateral PM. Collectively, this study provides support for a model in which fluid secretion is optimized after expression of K channels specifically in the apical PM.

The Journal of General Physiology

INTRODUCTION

The major physiological function of parotid acinar cells is the production of saliva, a watery fluid containing electrolytes and a complex mixture of proteins (Cook et al., 1994; Melvin et al., 2005). The driving force for fluid and electrolyte secretion is the vectoral, trans-epithelial movement of Cl^-. Cl^- is accumulated intracellularly via the concerted effort of several transporters, and after gustatory and olfactory stimulation, Cl^- exits into the lumen of the gland (Cook et al., 1994; Melvin et al., 2005). Sensory stimulation results in the release of acetylcholine from parasympathetic nerves and subsequently activates a signaling cascade, which ultimately causes an increase in the intracellular free calcium concentration $[Ca^{2+}]_i$ (Putney, 1986). The widely accepted model explaining the molecular mechanism underlying the secretion of the primary acinar cell fluid posits that Ca^{2+} plays a pivotal role in the activation of two major effectors absolutely required for saliva secretion (Putney, 1986). Of primary importance is the activation of a Ca^{2+}-activated Cl^- conductance, recently identified as a member of the TMEM16a gene family (Schroeder et al., 2008; Yang et al., 2008; Romanenko et al., 2010a). This channel is known to be localized to the apical plasma membrane (PM) and provides the route for Cl^- exit to the lumen (Yang et al., 2008; Romanenko et al., 2010a). Notably, Ca^{2+} also activates K channels that are members of the large-conductance "maxi-K" (BK; $K_{Ca}1.1$) and intermediate K (IK; $K_{Ca}3.1$) families (Maruyama et al., 1983; Wegman et al., 1992; K. Park et al., 2001; Nehrke et al., 2003; Begenisich et al., 2004; Romanenko et al., 2007). These channels are crucial to maintaining the acinar cell membrane potential ensuring the electrochemical driving force for Cl^- exit. Ultimately, fluid secretion occurs as cations, primarily Na^+, are drawn paracellularly through tight junctions into the lumen as a function of the trans-epithelial negative potential established by Cl^- efflux. Water then follows the osmotic potential and forms the primary acinar cell secretion. This fluid is thought to reflect the Na^+, K^+, and Cl^- composition of the interstitial fluid bathing the basolateral surface of the acinar cells. The final composition of saliva is substantially modified in the duct and results in a hypotonic solution, relatively low in Na^+ and Cl^- and conversely high in K^+ and HCO_3^- (Cook et al., 1994; Melvin et al., 2005).

Correspondence to David I. Yule: David_Yule@urmc.rochester.edu

Abbreviations used in this paper: BK, large-conductance "maxi-K"; $[Ca^{2+}]_i$, intracellular free calcium concentration; IK, intermediate K; $InsP_3$, inositol 1,4,5-trisphosphate; PM, plasma membrane; ZO-1, Zona occludens-1.

The Rockefeller University Press $30.00
J. Gen. Physiol. Vol. 139 No. 2 121–133
www.jgp.org/cgi/doi/10.1085/jgp.201110718

Although it is clear that that the Cl^- exit pathway must reside in the apical PM, most current models suggest that the K^+ conductance is present in the basal and lateral PM of the salivary acinar cell (Nauntofte, 1992; Turner et al., 1993; Turner and Sugiya, 2002; Gin et al., 2007). Indeed, numerous electrophysiological studies have detailed single K channel activity in patch-clamp studies of presumably basolateral PM (for example, see Maruyama et al., 1983). Consistent with this idea, simultaneous imaging of $[Ca^{2+}]_i$ and Ca^{2+}-activated K^+ current indicates that the activation of the K^+ current in submandibular cells coincided temporally with a rise in $[Ca^{2+}]_i$ in the basal aspects of the cell (Harmer et al., 2005). Micropuncture studies of salivary glands of various species indicate that although the $[K^+]$ in the primary saliva is somewhat higher than the interstitium, it is nevertheless lower than in the final saliva (Mangos and Braun, 1966; Mangos et al., 1966; Young and Schögel, 1966; Mangos and McSherry, 1969). Collectively, these data imply that K^+ secretion occurs primarily as a function of K channels expressed in the apical membrane of ductal cells (Nakamoto et al., 2008) and, moreover, that K channels are not present in great abundance in the apical membrane of submandibular acinar cells.

However, despite the current lack of definitive evidence, there are no inherent theoretical obstacles for the expression of at least a proportion of K channels in the apical PM to function to facilitate the hyperpolarized membrane potential necessary for Cl^- secretion from salivary glands. Indeed, contrary to studies in submandibular glands, reports have suggested that a high density of BK channels are present in the apical membrane of lacrimal acinar cells (Tan et al., 1992) and contribute to electrolyte secretion in this gland. A similar apical localization of BK channels has also been reported in exocrine glands from frog skin (Sørensen et al., 2001), lung (Manzanares et al., 2011), and in mammary gland epithelia (Palmer et al., 2011). Furthermore, an early electrical steady-state model of a polarized secretory epithelia suggested that an efficient fluid secretion could be achieved and indeed favored with K channels in the apical membrane (Cook and Young, 1989). In addition, a recent comprehensive dynamic mathematical model of salivary gland secretion, constructed to investigate how the distribution of K and Cl channels affects saliva secretion from parotid gland after an increase in $[Ca^{2+}]_i$, suggests that saliva is most efficiently produced when a portion of the K^+ conductance is localized to the apical membrane (Palk et al., 2010).

To specifically address the prediction made by these mathematical models, we have designed experiments to explicitly investigate whether K channels are functionally localized to the extreme apex of parotid acinar cells. Using a combination of whole cell patch-clamp electrophysiology together with spatially localized manipulation of $[Ca^{2+}]_i$, we demonstrate that both IK and BK channels exist in the apical PM of parotid acinar cells. Further, our data are consistent with the expression of a much higher density of channels in this domain than in the basolateral PM. These findings provide evidence to support the idea that an apical distribution of a portion of the complement of K channels may optimize stimulated fluid secretion from the parotid gland.

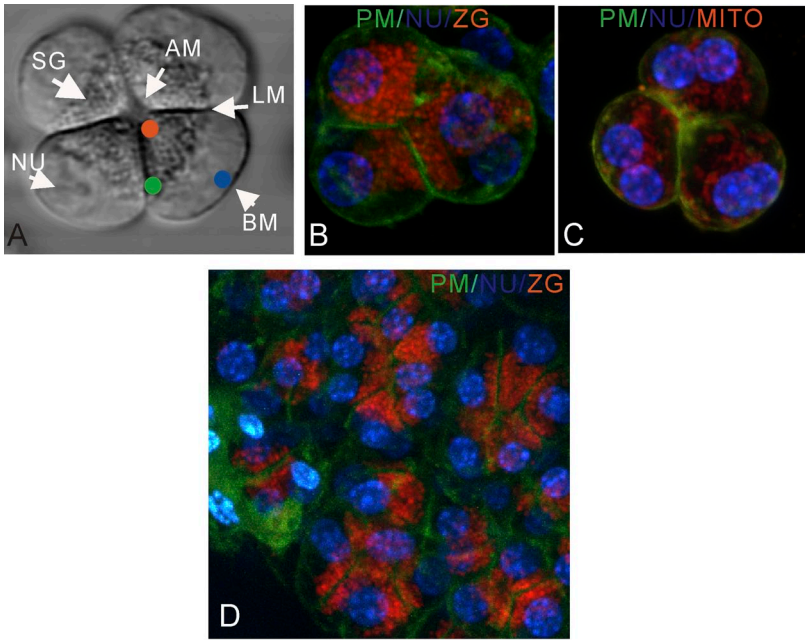

Figure 1. Polarized morphology of parotid acini. (A) A transmitted laser light image is shown of a small group of cells characteristic of those used throughout this study. The positions of secretory granules (SG), nucleus (NU), apical membrane (AM), lateral membrane (LM), and basal membrane (BM) are annotated. The position of apical (red dot), lateral (green dot), and basal (blue dot) photolysis sites is shown. (B) A maximum projection image, constructed from a z-series, is shown from a small group of cells stained with live cell markers of the nucleus (blue), granules (red), and PM (green). (C) A similar triplet was stained to indicate PM (green), nucleus (blue), and mitochondria (red). (D) Similar staining was performed in a parotid lobule not subjected to enzymatic digestion and indicates the similar localization of granules (red), PM (green), and nuclei (blue).

MATERIALS AND METHODS

Materials

Fluo-4 K^+ salt, NP EGTA ("caged Ca^{2+}"), Diazo-2 ("caged chelator"), MitoTracker red/green, LysoTracker red/green, FM-143, and trypsin were purchased from Invitrogen. Liberase TL was from Roche, and all other materials were from Sigma-Aldrich.

Parotid acinar cell preparation

Two types of mice were used in this study. The standard strain was C57B6, and we also used mice in which the gene encoding the BK channel was disrupted ($Slo^{-/-}$) (Meredith et al., 2004). Detailed descriptions of the procedures for tissue dissociation and parotid acinar cell preparation have been described previously (Won and Yule, 2006; Won et al., 2007). In brief, parotid glands were removed from 2–3-mo-old mice, finely minced, and digested for 8 min using 28 µg/ml trypsin. Tissue was then further dissociated for 1 h in 0.18 Wünsch units/ml Liberase and gently agitated to gain single and small clumps of acinar cells. Finally, parotid cells were filtered through 53-µm nylon mesh, washed, collected by centrifugation (3 min at 200 *g*), resuspended in media, and plated onto glass coverslips. All solutions were gassed continuously with 95% O_2 + 5% CO_2 and maintained at 37°C.

Experiments were performed on single or small clumps of parotid cells with pronounced polarized apical secretory granule localization. To meet this criterion, granules were tightly localized to the apical third of individual cells. An annotated bright field image of a small group of parotid acinar cells is shown in Fig. 1 A, which illustrates the polarized features of this cell type. Several preparations were also stained with live cell markers of nuclei (Hoechst), mitochondria (MitoTracker), granules (LysoTracker), and PM (FM-143) and imaged with confocal microscopy. As illustrated in Fig. 1 (B and C), cells typically retained polarized morphology characterized by apical granules, basal nuclei, perinuclear mitochondria, and bleb-free PM for ∼2 h after harvest. These characteristics were also evident in lobules of parotid gland not subjected to enzymatic digestion (Fig. 1 D). In addition, our previous studies have shown that cells used during this period are functionally polarized in that they retain apical-basal Ca^{2+} waves upon secretagogue stimulation or inositol 1,4,5-trisphosphate ($InsP_3$) uncaging (Giovannucci et al., 2002; Won et al., 2007). Procedures for animal handling, maintenance, and surgery were approved by the University of Rochester Committee on Animal Resources. All animals used in this study were housed in a pathogen-free area at the University of Rochester.

Immunofluorescence localization

Clumps of parotid acinar cells seeded on coverslips were fixed with ice-cold methanol. Somewhat larger acini were prepared for these experiments to more effectively visualize the acinar architecture, in particular, the highly elaborated luminal domain reported previously in salivary glands (Matsuzaki et al., 1999; Larina and Thorn, 2005). These acini were probed with antisera raised against BK (α-MSlo clone L6/60 monoclonal antibody; UC Davis, NeuroMab facility), α-K_{Ca}1.1 (Alomone Labs), α-type–3 $InsP_3$ receptor (BD), and Zona occludens-1 (ZO-1; Invitrogen) and subsequently with Alexa Fluor 488/568 (Invitrogen) secondary antibodies as indicated. The IK antibody was a rabbit polyclonal raised against the MIK 3,4 extracellular loop (peptide: RSPHCALAGEATDAQPWPGFL-GEGEC) and generated by Pocono Rabbit Farms. The localization was visualized using confocal microscopy on a microscope (Fluoview 1000; Olympus) equipped with a suite of diode and gas lasers.

Spatially limited flash photolysis, Ca^{2+} imaging, and electrophysiological recording

Whole cell currents were acquired at room temperature using an amplifier (Axopatch 200A) and digitizer (Digidata 1322A; both from Axon Instruments) at a 50-kHz sampling rate and filtered online at 5 kHz with a low-pass Bessel filter. Data acquisition was performed using pClamp 9 software package (Axon Instruments). During continuous current recordings, cells were voltage clamped at a holding potential of +40 mV (in I_{K+} recordings) or −20 mV (in I_{Cl^-} recordings). Pipettes of 6–8-MΩ resistance were used with the intracellular solution containing (in mM): 135 K-glutamate, 10 HEPES, 10 NP EGTA, 2 or 5 $CaCl_2$, and 250 µM Fluo-4 K, pH 7.2 (free $[Ca^{2+}]$ was ∼40 or ∼160 nM, respectively, estimated using Maxchelator); or 135 K glutamate, 10 HEPES, 2.5 Diazo-2, 10 EGTA, 7.53 or 8.6 $CaCl_2$, and 250 µM Fluo-4 K, pH 7.2 (estimated free $[Ca^{2+}]$ was 500 nM or 1 µM). The $[Ca^{2+}]$ of the pipette solutions was verified fluorimetrically. However, the measured $[Ca^{2+}]$ in the Diazo-2 solutions was unexpectedly lower than predicted (∼175 and ∼550 nM, 7.53 and 8.6 mM added $CaCl_2$, respectively). It is possible that this discrepancy reflects the presence of noncaged Ca^{2+} chelator in the solution. After patch rupture, 4 min was allowed for sufficient pipette solution equilibration. Because there is evidence that Ca^{2+}-activated Cl channels are exclusively localized in the apical region of acinar cells (M.K. Park et al., 2001; Yang et al., 2008; Romanenko et al., 2010a), the Cl^- current was used as positive control to validate photolysis at the apical region. External solutions were designed to isolate Ca^{2+}-dependent K^+ and Cl^- currents. For monitoring K channel currents, a solution with a very low Cl^- concentration was used. This solution contained (in mM): 135 Na-glutamate, 5 K-glutamate, 2 $CaCl_2$, 2 $MgCl_2$, and 10 HEPES, pH 7.2. To isolate particular Ca^{2+}-activated K^+ currents, the specific BK channel inhibitor paxilline or IK channel inhibitor TRAM-34 was present in the bath solution. Cl^- channel currents were measured after block of K channels with TEA. This solution consisted of (in mM): 140 TEA-Cl and 10 HEPES, pH 7.2.

Changes in Fluo-4 fluorescence were monitored using a monochromator-based imaging system (Polychrome IV) and high-speed CCD camera (both from TILL Photonics). Cells were illuminated at 488 nm, and fluorescence was collected through a 525-nm band-pass filter (Chroma Technology Corp.). Images were acquired at 45–52-ms intervals depending on image size, with an exposure of 20 ms and 2 × 2 binning, and displayed as $\Delta F/F_0 = (F - F_0)/F_0$, where F was the recorded fluorescence and F_0 was the average fluorescence of the initial 10 sequential frames of the image series. Images were scaled to 4,096 gray levels and pseudocolored.

Flash photolysis of caged compounds was performed using a UV laser and custom-designed condenser, as described previously in detail (Won et al., 2007). In brief, a 375-nm diode laser (maximum output, 18 mW; Toptica) was interfaced to an inverted microscope (TE200; Nikon) through a single-mode fiber and a dual-port UV flash condenser (TILL Photonics). The laser was brought to focus in the sample plane using a ×40 (NA = 1.3) oil-immersion objective (Nikon). The full width at half-maximum of the laser point was ∼0.7 µM in the x and y plane and ∼2.0 µm in the z plane. Previous modeling suggested that 70% of the optical power is contained inside a spot of 1-µm diameter (Won et al., 2007). The laser power was software controlled between 0.5 and 6 mW, and the cells were illuminated for one image frame (i.e., between 45 and 52 ms). The whole cell current recordings, fluorescence image acquisition, and triggering of the laser exposure were synchronized by the Polychrome IV image controller and executed by the Vision suite of software (TILL Photonics).

Experiments were performed using varied Ca^{2+} buffering to establish suitable conditions to result in spatially localized Ca^{2+} elevations after photolysis of caged Ca^{2+}. The laser emission was positioned next to the appropriate PM, and Ca^{2+} release was deemed local if the change in fluorescence measured on the opposite pole of the cell remained less than a 10% increase over the resting signal in this region (i.e., $\Delta F/F_0 < 1.1$). Initial trials were

performed in cells loaded with 10 mM NP EGTA and 5 mM $CaCl_2$ (free Ca^{2+}, ~160 nM). As shown in Fig. 2 (A, images, and B, kinetic traces immediately after the flash from either apical [red] or basal [blue]), under these conditions, large Ca^{2+} transients were evoked that were not spatially limited to the appropriate region. In an effort to spatially constrain the Ca^{2+} signal, the buffering capacity was enhanced by increasing the NP EGTA-Ca^{2+} ratio. Fig. 2 (C, images, and D, kinetic) shows a representative experiment in cells dialyzed with 10 mM NP-EGTA and 2 mM Ca^{2+} and demonstrates that, under these conditions, a sizeable Ca^{2+} transient could be generated without significant spread of the signal away from the photolysis site. In this example, the laser was focused on the apex of the cell (Fig. 2 C, red spot). Fig. 2 E illustrates a typical example of the image of a peak post-flash fluorescence change and the spatial analysis of the change in fluorescence along a line from the photolysis site in the apical region to the basal PM. Fig. 2 F shows normalized pooled data from several experiments. This analysis demonstrates that the increase in fluorescence peaks 0.46 ± 0.13 µm from the center of the flash site (pixel size, 0.32 µm) and decays exponentially from the photolysis site with a mean length constant of 2.5 ± 0.2 µm (average cell diameter, 14.1 ± 0.81 µm). These data demonstrate that laser exposure under these buffering conditions results in minimal changes in fluorescence in the basal aspects of the cell and was therefore adopted in all subsequent caged Ca^{2+} photolysis experiments. A similar approach to producing a spatially limited Ca^{2+} reduction after photolysis of the caged chelator Diazo-2 was used for experiments described in Fig. 5.

Data analysis

Data were analyzed with Origin software (OriginLab). Data are expressed as mean ± SEM of *n* independent experiments. Statistical comparisons were by paired Student's *t* test. $P < 0.05$ was considered statistically significant.

Online supplemental material

Fig. S1 depicts photolysis of caged Ca^{2+} on more lateral aspects of the PM. Identical methods detailed in the text associated with Figs. 1–4 were used for these experiments. Fig. S1 is available at http://www.jgp.org/cgi/content/full/jgp.201110718/DC1.

RESULTS

Our first series of experiments was performed to investigate if Ca^{2+}-activated K channels are expressed in the extreme apical domain of parotid acinar cells. Data were collected from single cells and small clumps with pronounced polarized morphology as defined in Fig. 1.

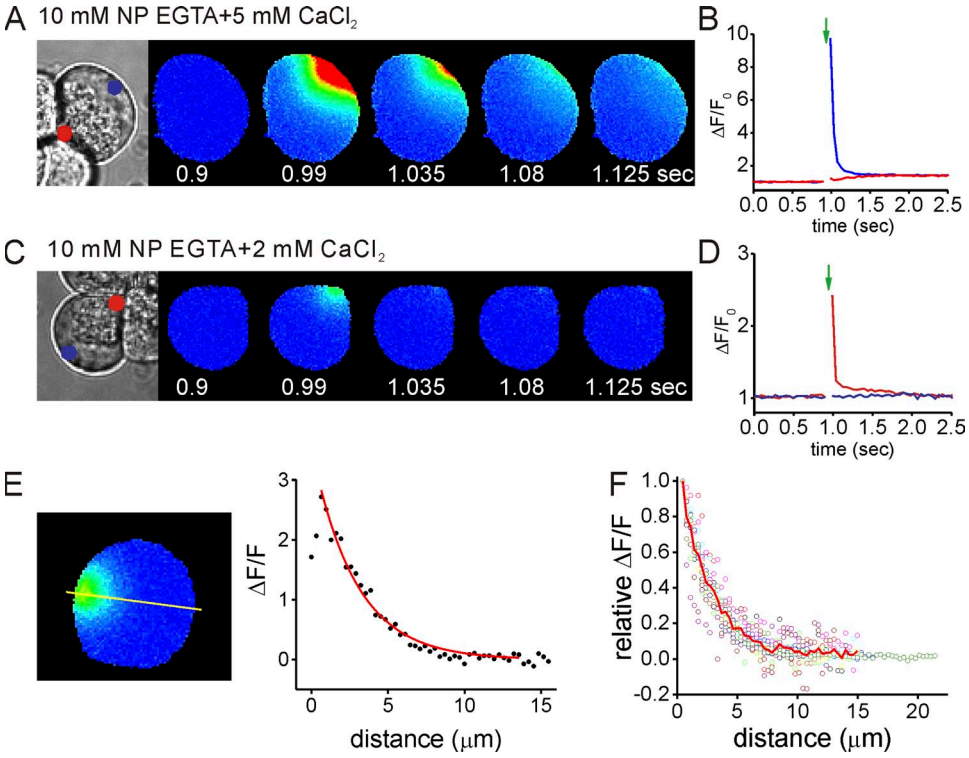

Figure 2. Establishing conditions for local manipulation of $[Ca^{2+}]$. (A) A bright field image of a parotid acinar cell is shown together with pseudocolored fluorescence image series of cells immediately before and after flash photolysis. The pipette solution contained 10 mM NP-EGTA and 5 mM Ca^{2+} (free Ca^{2+}, ~160 nM). The images were acquired every 45 ms, and the single image containing the flash artifact was removed. Release of Ca^{2+} after laser exposure (green arrow) resulted in a marked increase in fluorescence at the photolysis site in the basal pole (blue dot), which decayed rapidly but spread toward the apical pole (red dot). (B) The change in $\Delta F/F_0$ ratio in either the basal (blue line) or apical (red line) region, demonstrating that the increase in the "untargeted" pole was >10% when compared with basal values. (C) A similar experiment is shown, except the pipette solution contained 10 mM NP-EGTA and 2 mM Ca^{2+} (free $[Ca^{2+}]$, ~40 nM). The series of images demonstrates that the increase in $[Ca^{2+}]$ remains localized to the apical pole (red dot) under these conditions. (D) The change in $\Delta F/F_0$ ratio values for this experiment, indicating that the marked increase in fluorescence after laser exposure in the apical domain (red line) results in little increase (<10% increase over basal) in fluorescence in the untargeted region (blue line). (E) A spatial analysis of the peak change in fluorescence after photolysis with buffering conditions as in C. The peak change in fluorescence shown in E (left) was compared with an average image generated from the previous five frames under basal conditions. The change in $\Delta F/F_0$ ratio along the yellow line is shown in the right panel and demonstrates that the fluorescence decays exponentially from the photolysis site, with a length constant of 2.5 ± 0.2 µm. The fit for the decay is shown in the red line. (F) A similar analysis in which the individual experiments are normalized to the peak fluorescence in the individual cell. The red line shows the mean fit of the data.

An example of this type of experiment is illustrated in Fig. 3. A bright field image of the small clump is shown in Fig. 3 A (left). The uppermost cell was attached to the recording pipette, which contained Ca^{2+} indicator dye and caged Ca^{2+} as described in Materials and methods. The UV laser was focused on the apical PM (at the position indicated by the red dot), and whole cell currents were monitored. Laser emission was initiated 1.05 s after the start of electrical recording as detailed in Materials and methods. An increase in the fluorescence signal was evoked, which peaked in the subsequent frame, reflecting an almost instantaneous rise in $[Ca^{2+}]_i$. A continuous recording of fluorescence in both the apical (red) and basolateral (blue) regions is shown in Fig. 3 B, with the time of the laser flash indicated by the green arrow. It is clear from these records that the increase in $[Ca^{2+}]$ was confined to the extreme luminal side of the cell. On average, the fluorescence change measured in the apical membrane region reached 3.03 ± 0.05 ($\Delta F/F_0$ range between 1.7 and 7.7; n = 12) and remained essentially unchanged (<10% increase over basal values; mean, 1.05 ± 0.01; $\Delta F/F_0$ range between 1.006 and 1.095) near the basal membrane.

Fig. 3 C (top) shows the whole cell K^+ currents recorded at +40 mV for approximately a second before and after the laser exposure (arrow). The basal $[Ca^{2+}]$ in the intracellular solution for these experiments was too low to significantly activate IK Ca^{2+}-activated K channels. The 40-mV recording voltage will activate parotid BK channels even in low $[Ca^{2+}]$, accounting for the large (near 1.7-nA) baseline level of K^+ current recorded before the laser flash. The local elevation of $[Ca^{2+}]_i$ resulted in a rapid rise in K^+ current of ~0.6 nA (mean current, 1.1 ± 0.11 nA preflash vs. 1.49 ± 0.16 nA postflash; P < 0.001; n = 12). The mean fractional increase in K channel current was 1.34 ± 0.02 (n = 12), indicating the presence of a significant number of K channels located in the apical region of the cells. Fig. 3 D (left) shows that an increase in apical K^+ current was observed in all 12 cells that were similarly tested.

Immunocytochemistry indicates that Ca^{2+}-activated Cl channels (TMEM16a) are only present in the apical membrane of salivary acinar cells (Yang et al., 2008; Romanenko et al., 2010a). Consistent with this idea, a similar approach to the current studies demonstrated that functional Ca^{2+}-dependent Cl channels are restricted to the apical membrane of pancreatic acinar cells (M.K. Park et al., 2001). We therefore used the presence of Ca^{2+}-activated Cl^- currents as an electrophysiological marker of the apical membrane. In several experiments, a second photolysis was performed at the same location, juxtaposed to the apical PM, after replacing the bath solution with one containing 140 mM TEA-Cl to inhibit K^+ conductances and to provide Cl ions. As illustrated in Fig. 3 C (bottom), the second laser exposure elicited a comparable Ca^{2+} increase to the first

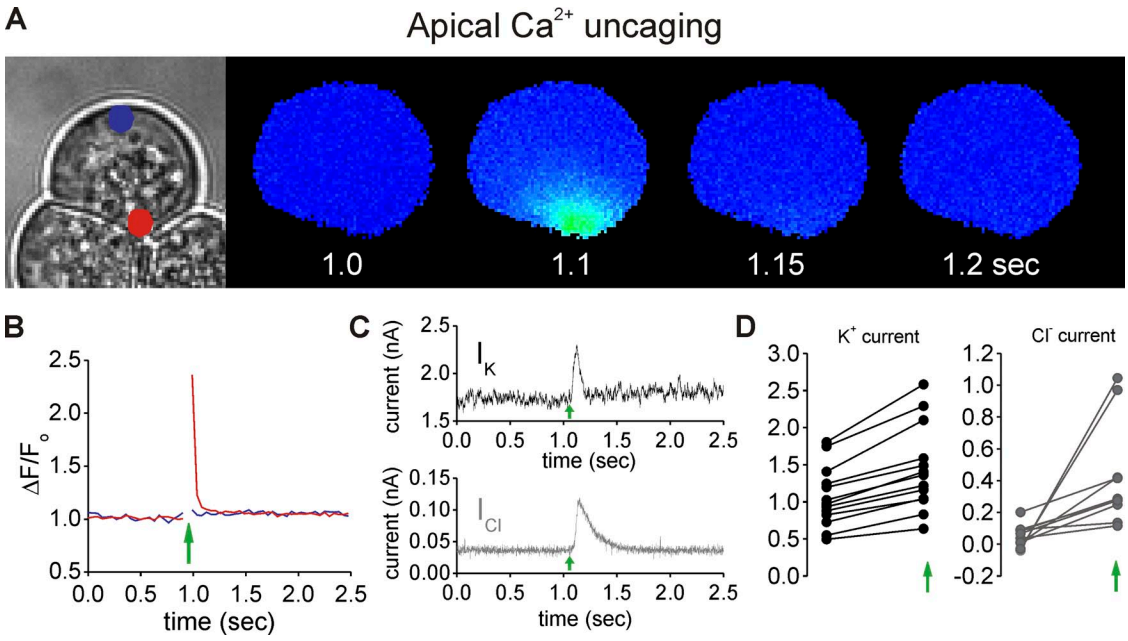

Figure 3. Apically localized increase in $[Ca^{2+}]$ activates K and Cl channels. Experiments were performed with the buffering conditions established in Fig. 2 (C–F). (A) A bright field and pseudocolored image series in which the $[Ca^{2+}]$ was increased close to the apical PM (red dot). (B) In these images and kinetic plot, a marked increase in signal was evoked in the apical domain (red line) and remained highly localized. A minimal increase is observed in the basal region (blue line) after laser exposure (green arrow). (C; top) The increase in whole cell K^+ current evoked by the Ca^{2+} transient in B is shown. (Bottom) The increase in Cl^- current after a subsequent apical laser exposure after the bath solution had been exchanged for 140 mM TEA-Cl. A robust increase in whole cell Cl^- current is evoked. (D)Paired experiments before and after flash.

exposure and an associated, large increase in Cl^- current (mean current, 0.05 ± 0.02 nA preflash vs. 0.42 ± 0.1 nA post-flash; $P < 0.01$; $n = 10$). The data in Fig. 3 D (right) show that an increase in Cl channel current was observed in all similar experiments. These data indicate that both Ca^{2+}-activated Cl and K channels share a similar distribution in the extreme apical region of parotid acinar cells.

The apical domain of exocrine cells is estimated to contribute between 3 and 8% of overall PM surface area (Poulsen and Bundgaard, 1994), and thus, on-cell patch-clamp studies monitoring K channels likely reflect K channels present in the basal and lateral PM. Indeed, we readily observed single-channel activity, consistent with BK currents in cell-attached patches, whose activity was increased by uncaging Ca^{2+} or carbachol application (not depicted). To investigate the contribution of K channels outside the apical domain, we next performed experiments with the laser positioned immediately below the PM on the basal side of parotid acinar cells. The local post-flash increase in $[Ca^{2+}]_i$ was comparable to the previous apical photolysis experiments (mean increase in $\Delta F/F_0$, 2.66 ± 0.38; range between 1.8 and 3.4) and remained highly localized (Fig. 4, A, images, and B, kinetic; mean rise in apical $\Delta F/F_0$, 1.04 ± 0.01; range between 1.01 and 1.07). Surprisingly, this increase in $[Ca^{2+}]$ did not result in any significant elevation in K^+ current (mean current, 1.25 ± 0.37 nA preflash vs.1.27 ± 0.39 nA post-flash; $n = 4$), as presented in Fig. 4 (C, top, and D, left). Subsequent photolysis in the same cells in TEA-Cl–containing solution also failed to evoke any Cl^- current, as shown in Fig. 4 (C, bottom, and D, right; mean current, 0.08 ± 0.04 nA preflash vs. 0.08 ± 0.04 nA post-flash; $n = 4$). These data confirm the localization of the laser exposure to the basal domain and furthermore substantiate the idea that apically localized channels were not exposed to any increase in $[Ca^{2+}]$ in these experiments. In several experiments using the same cells, the laser power was increased in an effort to evoke a larger increase in $[Ca^{2+}]$. In these experiments, the change

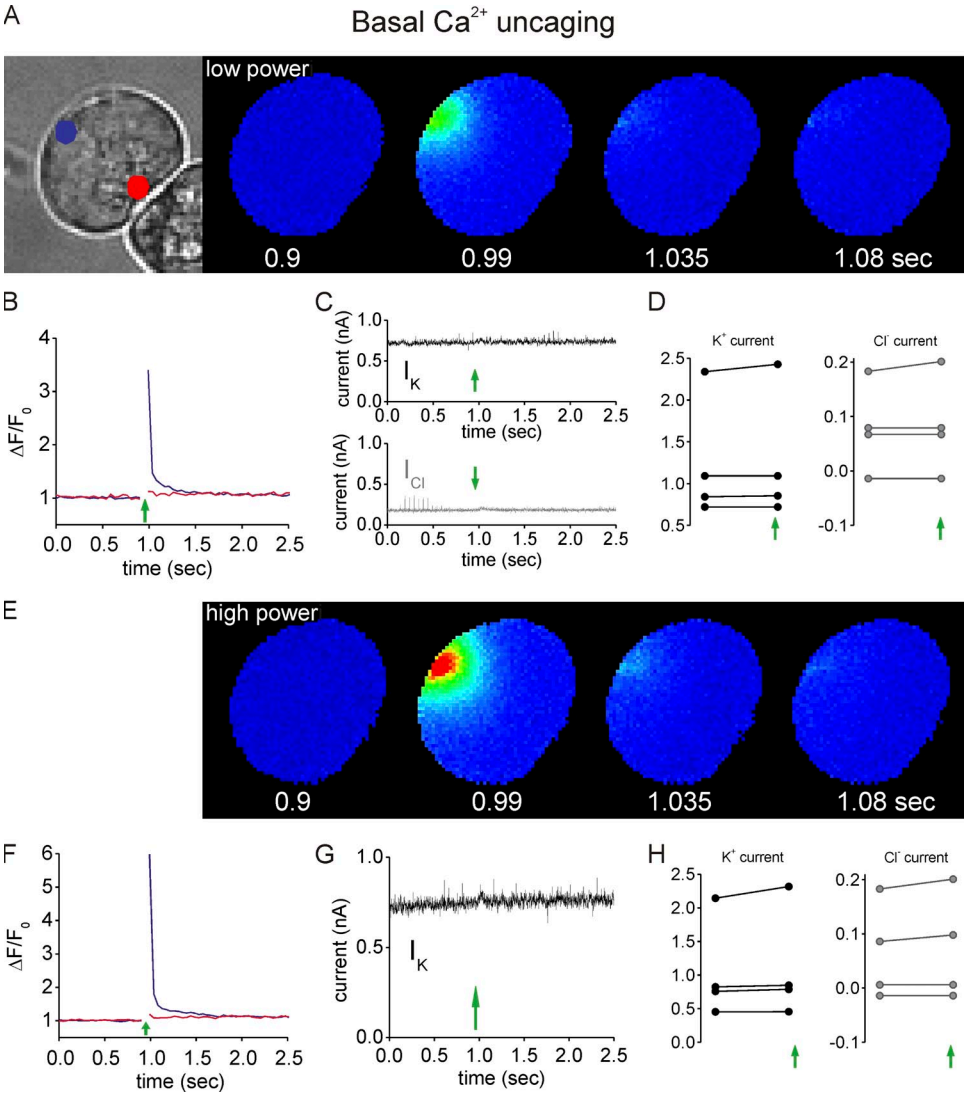

Figure 4. Basolaterally localized increases in $[Ca^{2+}]$ fail to activate K and Cl channels. (A) A bright field and pseudocolor image series is shown for a cell in which $[Ca^{2+}]$ was increased under the basal PM (blue dot) using laser parameters identical to Fig 3. (B) The kinetic demonstrates that a substantial and localized increase in fluorescence was evoked. Increasing the $[Ca^{2+}]$ at the basal PM failed to significantly activate K channels (C, top) or Cl channels in TEA-Cl solution (C, bottom). (D) Paired experiments before and after flash. (E) Similar experiments were performed, but the laser power output was increased to generate a larger increase in $[Ca^{2+}]$, as shown in E (images) and F (kinetic). (G) Under these conditions, no increase in K^+ conductance could be evoked. (H) Paired experiments demonstrating that no significant increase in either K^+ (left) or Cl^- (right) conductance occurred under these conditions.

in local $\Delta F/F_0$ ratios at the basal PM was substantially higher (Fig. 4, E, images, and F, kinetic; mean change in $\Delta F/F_0$, 6.21 ± 1.95; range between 3.18 and 11.79) and was less tightly localized, as a small but measurable increase in fluorescence could be measured in the apical pole (mean $\Delta F/F_0$ change, 1.16 ± 0.04; range between 1.09 and 1.27). Despite the larger, less localized $[Ca^{2+}]$ change, no statistically significant increase in K^+ current was evoked (mean current, 1.04 ± 0.38 nA preflash vs. 1.1 ± 0.41 nA post-flash; $n = 4$; Fig. 4, G and H, left). Similarly, in TEA-Cl–containing solutions, no increase in Cl^- current could be demonstrated (mean current, 0.07 ± 0.04 nA preflash vs. 0.07 ± 0.05 nA post-flash; $n = 4$; Fig. 4 H, right). The latter finding indicates that although less localized, the increase in $[Ca^{2+}]$ evoked by greater laser exposure is still not sufficient to activate apically localized channels and serves to validate the more conservative inclusion parameters for localized signals used in Figs. 2 and 3.

Next, we addressed if K^+ currents could be evoked by local uncaging in the more lateral aspects of parotid acinar cells. Morphologically, we defined the lateral PM as the peripheral membrane on an arc approximately equidistant from the extreme apical and basal regions. Functionally, this membrane was again defined by the absence of Ca^{2+}-activated Cl^- currents. In four cells, the K^+ conductance before uncaging was 0.904 ± 0.115 nA and did not significantly change after photo-release of Ca^{2+} (0.915 ± 0.11 nA post-flash; mean change in $\Delta F/F_0$ = 1.99 ± 0.193–fold over baseline; range, 1.5–2.3). In these cells, the Cl^- was also unchanged after photolysis (0.073 ± 0.01 nA before and 0.075 ± 0.01 nA after photolysis). Notably, in four additional experiments, small K^+ and Cl^- currents were evoked after similar highly localized, presumed lateral photolysis (I_K, 0.946 ± 0.055 nA before and 1.023 ± 0.039 nA after photolysis; I_{Cl}, 0.166 ± 0.027 nA before and 0.208 ± 0.03 nA after photolysis). These data are presented in Fig. S1. Our interpretation of these data is that when currents were evoked that this actually represents activation of K and Cl channels in the extended luminal membrane. Further, these data indicate that although lateral PM is morphologically distinct, it is, as expected, functionally very similar to the basal PM. This conclusion is consistent with immunocytochemical localization of TMEM16A (Romanenko et al., 2010a) and tight junction markers, which suggest that salivary glands have a relatively elaborate and enlarged luminal membrane structure (Matsuzaki et al., 1999; Larina and Thorn, 2005). This organization has been proposed to represent a specialization of the gland to facilitate copious fluid secretion.

To further test the hypothesis that K channels are expressed in the apical domain of parotid acinar cells, a complimentary approach was designed whereby the activity of K channels preactivated by elevated $[Ca^{2+}]_i$ was monitored after focal release of the caged Ca^{2+} chelator, Diazo-2. Experiments were performed with a pipette solution with either ∼175 or ∼550 nM Ca^{2+}. These $[Ca^{2+}]$ have been shown previously to activate BK and IK channels in parotid acinar cells (Romanenko et al., 2010b). Again, we empirically determined that a localized, pole-specific reduction in $[Ca^{2+}]_i$ could be achieved after brief, low power laser exposure by inclusion of 2.5 mM Diazo-2 in the patch pipette. Fig. 5 shows a representative experiment in which the cell was initially dialyzed with 550 nM Ca^{2+} before photolysis of Diazo-2 in the apical pole (A, images, and B, kinetic). Spatial analysis, comparing the change in fluorescence along an axis from the apical to basal pole in pre- and post-flash images, confirmed that the decrease is highly localized and decayed exponentially from the laser exposure point with a length constant of 3.63 ± 0.27 µm (Fig. 5 C; $n = 9$). This decrease in $[Ca^{2+}]$ in the apical pole was sufficient to significantly reduce the K^+ current in all nine cells in which this experiment was performed and provides further support for our contention that K channels are present in the apical PM. Based on the initial correlation of the currents and Ca^{2+} signal, we analyzed the reduction in currents at the peak of the Ca^{2+} signal decline. The average K^+ current reduction was 118 ± 25 pA (Fig. 5, D, top, and E, left, high $[Ca^{2+}]$; $P < 0.001$). A second exposure to laser illumination in cells, now bathed in TEA-Cl, also resulted in a significant reduction in Cl^- current on average 95 ± 20 pA ($n = 8$), confirming the apical localization of the conductance monitored (Fig. 5, D, bottom, and E, right, high $[Ca^{2+}]$; $P < 0.01$). Similar experiments were performed in cells dialyzed with a pipette solution containing 175 nM Ca^{2+}. Although the amount of baseline current was reduced in these experiments, apical photolysis of Diazo-2 again resulted in a statistically significant decrease in both K^+ current (Fig. 5 E, right, low $[Ca^{2+}]$) and Cl^- current (Fig. 5 E, left, low $[Ca^{2+}]$).

It should be noted that in a majority of trials (seven of nine experiments), both the K^+ and Cl^- currents, although closely tracking the initial decrease in $[Ca^{2+}]$ after the flash, smoothly attained a sustained lower level. Although the $[Ca^{2+}]$ signal had a large transient component, the Ca^{2+} level remained somewhat reduced after the flash and likely accounted for the sustained change in current level. The lack of complete recovery of the Ca^{2+} signal might result from a relatively maintained level of Ca^{2+} chelator after the flash. The lack of a rapid transient change in channel activation may reflect several factors, including the fact that the high initial $[Ca^{2+}]$ concentration may have fully activated the channels leading to complex kinetics for Ca^{2+} binding to, and activation of, the channel.

Experiments were also performed to locally reduce the $[Ca^{2+}]_i$ in the extreme basal pole of parotid acinar cells dialyzed with a pipette solution containing 550 nM $[Ca^{2+}]$. Again, a local, pole-specific reduction in $[Ca^{2+}]_i$ was readily

achieved after laser exposure (Fig. 5, F, images, G, kinetic, and H, spatial analysis). Despite the reduction in fluorescent signal, and thus presumably the $[Ca^{2+}]$ being comparable in both poles, in this series of experiments, no change in K^+ current or Cl^- current was observed after basal photolysis of Diazo-2 (Fig. 5, I and J, $n = 5$ or 3 K^+ or Cl^-, respectively). These data are again consistent with the proposal that K channels are present in the apical pole at a denser distribution relative to the basal aspects of parotid acinar cells.

Next, experiments were performed to define which class of Ca^{2+}-activated K channel contributes to the apical K^+ current observed in the previous experiments. Initially, a pharmacological approach was taken using relatively specific chemical inhibitors of BK and IK and monitoring their effects on the K channel activity after a focal increase in apical $[Ca^{2+}]$ as defined in Figs. 2 and 3. The BK channel inhibitor paxilline or IK channel inhibitor TRAM-34 was bath applied at 1 μM, a concentration shown previously to maximally inhibit

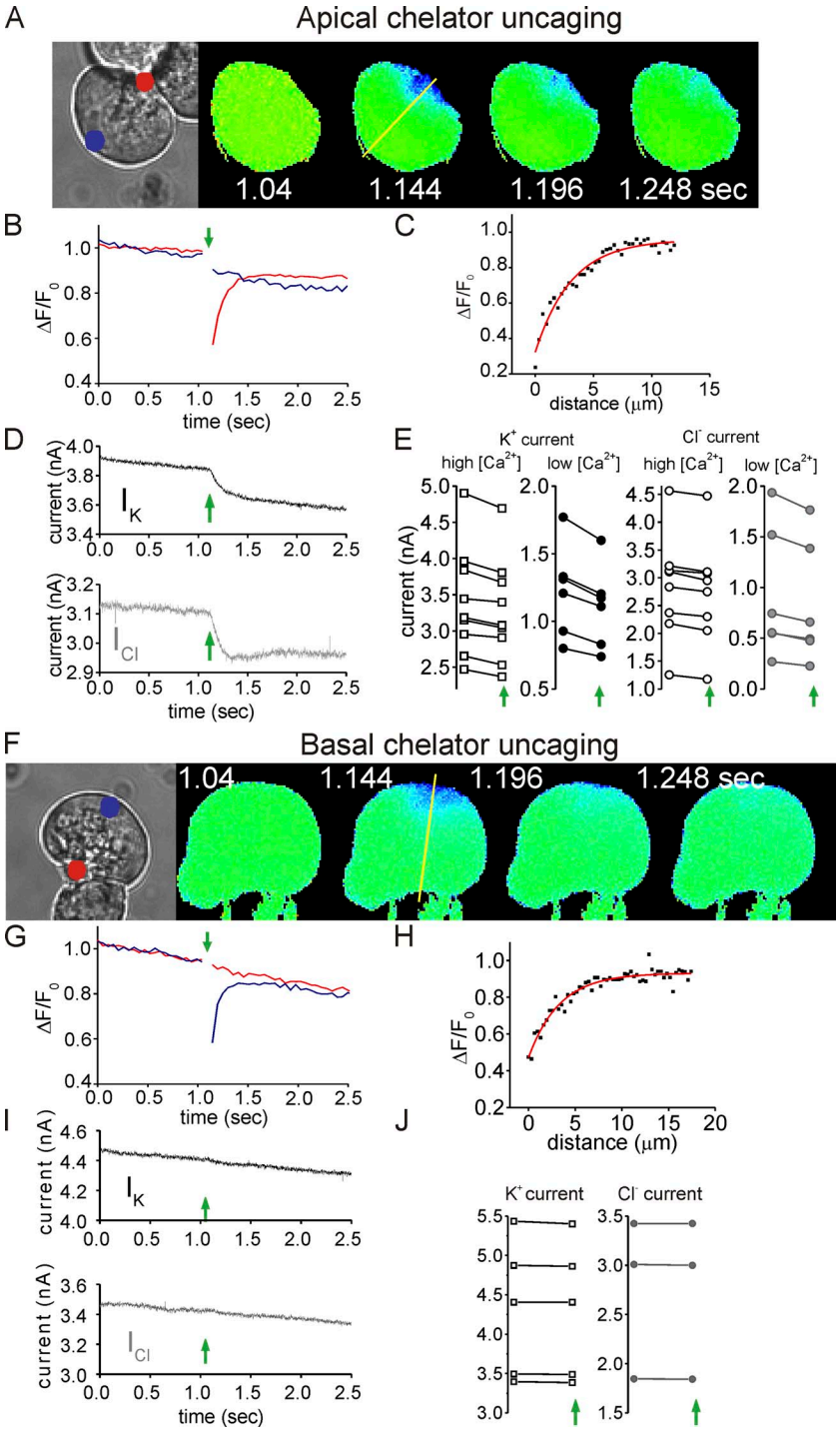

Figure 5. An apical reduction in $[Ca^{2+}]$ reduces the activity of K and Cl channels. Local photolysis of Diazo-2 was used to reduce the $[Ca^{2+}]$ specifically at either the basal or apical pole in cells dialyzed with Ca^{2+} to preactivate Ca^{2+}-sensitive currents. (A) A bright field and pseudocolored image series is shown from a cell dialyzed with ~550 nM $[Ca^{2+}]$. After laser exposure, the fluorescence decreased specifically in the apical pole. (B) The kinetic showing the decrease in fluorescence after laser exposure in the apical pole (red line) and basal pole (blue line). (C) The spatial analysis along the yellow line of the peak change in fluorescence compared with the mean of the five previous basal frames. The single-exponential fit is shown in the red line, and the mean of these analysis yields a length constant of 5.02 ± 0.76 μm. (D; top) The decrease in $[Ca^{2+}]$ evoked in A resulted in a significant reduction in K^+ and Cl^- conductance (bottom). (E) Paired experiments are shown before and after flash for either 550 or 175 nM $[Ca^{2+}]$, "high" or "low" $[Ca^{2+}]$, respectively. In F (images) and G (kinetic), basal photolysis of Diazo-2 resulted in a similar decrease in $[Ca^{2+}]$ in the basal domain, which again remained localized as demonstrated by the spatial analysis shown in H. (I and J) Basal photolysis failed to reduce either K^+ or Cl^- currents in cells dialyzed with the "high $[Ca^{2+}]$" pipette solution.

the respective channels (Romanenko et al., 2007). Importantly, both compounds act in a Ca^{2+}-independent manner (Strøbaek et al., 1996; Wulff et al., 2000). The baseline levels of K^+ current in the presence of paxilline before an increase in $[Ca^{2+}]$ in Fig. 6 A were very small (mean preflash current, 0.095 ± 0.01 nA; $n = 3$) and are consistent with most of the K^+ currents recorded in the absence of paxilline arising from BK channels, as was discussed in the text associated with Fig. 3. Also consistent with this conclusion is that the baseline currents in the presence of TRAM-34 were only slightly smaller than in the absence of this IK channel inhibitor (mean preflash current, 0.88 ± 0.09 nA; compare Fig. 3 D). The data in Fig. 6 A illustrate the observed flash-induced increase in K channel currents in the presence of TRAM-34 (left, $n = 6$) or paxilline (right, $n = 3$). The increase in current in the presence of each inhibitor demonstrates that both types of channels responded to the increase in apical $[Ca^{2+}]$. Consistent with this idea, inclusion of both inhibitors essentially abolished the current evoked by apical photolysis (Fig. 6 A, right, $n = 3$).

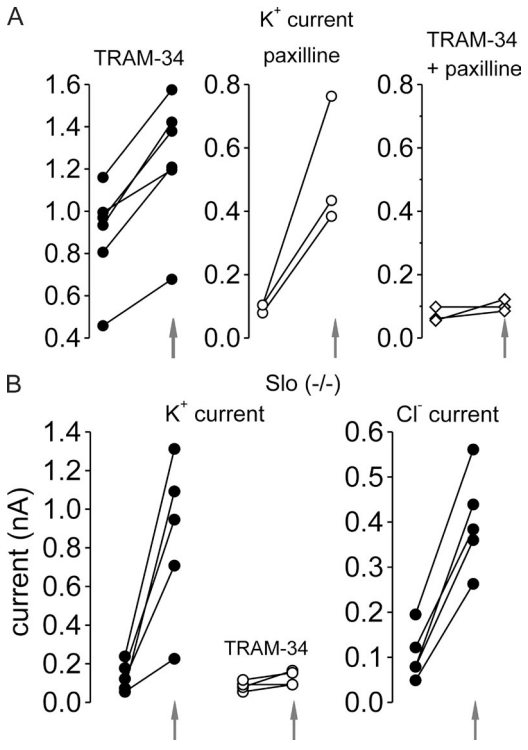

Figure 6. BK and IK are present in the apical PM. Experiments were performed using the techniques described in Fig. 3 to analyze the contribution of IK and BK to the currents evoked by apical photolysis. (A) K^+ currents could be evoked in the presence of either TRAM-34 (left) or paxilline (middle) but were essentially abolished when cells were incubated with both agents. (B) Similar experiments were performed in BK-null animals ($Slo^{-/-}$). The baseline current was reduced, but apical photolysis resulted in an increase in the remaining IK current, which was markedly reduced in the presence of TRAM-34. However, Cl^- currents could be evoked by apical photolysis in the same cells (right).

To further probe the contribution of apical IK channels, experiments were performed in transgenic BK-null mice (Meredith et al., 2004). In parotid acinar cells isolated from these animals, an apical increase in $[Ca^{2+}]$ evoked a large increase in K^+ current (mean current, 0.133 ± 0.03 nA preflash vs. 0.857 ± 0.186 nA post-flash; $n = 5$) and Cl^- current (mean current, 0.105 ± 0.025 nA preflash vs. 0.401 ± 0.049 nA post-flash; $n = 5$). Notably, in a similar fashion to wild-type animals, basal photolysis failed to evoke an increase in K^+ current (not depicted). The increase in K^+ current after apical photolysis was almost abolished by exposure to TRAM-34 (Fig. 6 B).

In a final series of experiments, we investigated the distribution of K channels by immunofluorescence techniques. Using a variety of antibodies raised against BK, we were unable to detect any specific distribution in clumps of parotid acinar cells. However, an antibody raised against IK showed prominent membrane localization, which appeared to be enriched in the apical portion of the cell (Fig. 7, B and F). This staining was completely abolished by preincubation with the peptide used to raise the antibody. A portion of the IK staining also colocalized with the tight junction marker ZO-1 (Fig. 7 C), indicating an apical distribution of a portion of IK channels. Furthermore, the apical PM staining colocalized with labeling of the $InsP_3R$-3 (Fig. 7 G,) which resides on specialized ER immediately below the apical PM (Nathanson et al., 1994; Lee et al., 1997a; Yule et al., 1997; Larina and Thorn, 2005). Notably, this localization data are again consistent with an extremely elaborated apical/luminal domain in salivary acinar cells. Collectively, these data strongly suggest that K channels are present and functional in the extreme apical portion of PM in parotid acinar cells.

DISCUSSION

The electrochemical driving force for Cl^- secretion and thus fluid secretion is maintained by the exit of K^+ from salivary acinar cells. Theoretically, K^+ could leave exclusively from the basolateral PM, apical PM, or by a distribution of K channels to both domains. Numerous models of epithelial fluid secretion have been based on K^+ exit exclusively through the basal membrane. Indeed, this is an intuitive assumption, based on the observation that the primary saliva is rich in Na^+ and not K^+. Furthermore, significant or exclusive localization of apical K channels has been suggested to likely impede secretion by resulting in a more depolarized basolateral PM. Basolateral PM depolarization would then decrease the activity of both the Na/K-ATPase and Na/K/2Cl transporter and ultimately lead to reduced intracellular Cl^- accumulation (Silva et al., 1977; Palk et al., 2010). Despite these ideas, alternative models have predicted that fluid secretion would be more effective if some K channels are implicitly located to the apical PM of salivary acinar

cells (Cook and Young, 1989; Palk et al., 2010). However, to date, little experimental data are available to support this idea in salivary acinar cells.

In this study, we have used a combination of whole cell electrophysiology and spatially restricted manipulations of intracellular [Ca^{2+}] to functionally investigate the distribution of K channels in parotid acinar cells. Importantly, we first established conditions using focal laser illumination of caged molecules, which allowed the [Ca^{2+}] to be selectively manipulated in a small volume under either the apical or basal PM. These parameters were verified by temporally resolved digital imaging and show minimal signal contamination outside the targeted compartment. Using this experimental paradigm, the primary finding of this study is that a localized, brief increase in [Ca^{2+}] after photolysis of caged Ca^{2+} directed to a volume in the extreme apex of a parotid acinar cell elicited a marked increase in K^+ conductance. Experiments using relatively specific pharmacology suggest that both BK and IK contribute to this conductance, and this co-distribution may reflect the intimate interaction that has been reported for these channels in parotid acinar cells (Thompson and Begenisich, 2006, 2009). Confirmation that the apical PM was specifically targeted was confirmed as a robust Cl^- current was always elicited by comparable apical photolysis in the same cells. Notably, an increase in Cl^- current was never evoked by basal photolysis. In addition, when the [Ca^{2+}] was transiently reduced under the apical PM from levels that activate IK and BK, the whole cell K^+ conductance was reduced. In total, the apical photolysis experiments combined with immunofluorescence localization of IK provide strong evidence that some K channels are distributed to a distinct compartment shared with Cl^- channels located in the extreme luminal domain of parotid acinar cells.

This conclusion does differ significantly from an earlier study performed in submandibular salivary gland acinar cells. Harmer et al. (2005) reported that Ca^{2+} signals evoked by either low concentrations of ACh or $InsP_3$ dialysis through the patch pipette could be localized and maintained in the apical domain. Notably, these localized signals selectively activated Cl^- currents, and only Ca^{2+} signals that spread to the basolateral face of the cell elicited any K^+ conductance. Although we have no explanation for these disparate findings, acinar cells from the two salivary glands have specific Ca^{2+}-signaling characteristics and distinct physiology, with parotid acinar cells being responsible for the major volume of stimulated saliva secretion. Moreover, local Ca^{2+} signals have not been reported in parotid acinar cells, and, in the absence of significant experimental intervention, signals invariably rapidly globalize (Giovannucci et al., 2002; Won et al., 2007). It is therefore possible that the specific localization of K channels represents specializations unique to the individual cell types.

Given the expectation supported by our immunofluorescence data that K channels are distributed throughout the acinar cell PM, a somewhat surprising finding is that similar experiments manipulating Ca^{2+} in the basal and lateral aspects of the cell failed to reveal a measurable K^+ current. However, these data do not exclude the presence of K channels above the tight junctional complexes of parotid acinar cells, but rather may indicate that the density of K channels is higher in the restricted area constituting the apical PM. In this scenario, our failure to activate this reduced density of K channels might be explained by an inability to generate a sufficiently large, but still localized, increase in $[Ca^{2+}]_i$ using these techniques. A further conclusion drawn from the fact that a K^+ conductance could not be evoked except by focal apical photolysis is that it appears unlikely that basal or lateral K channels are at sufficient density to contribute to the increase in conductance observed after apical photolysis.

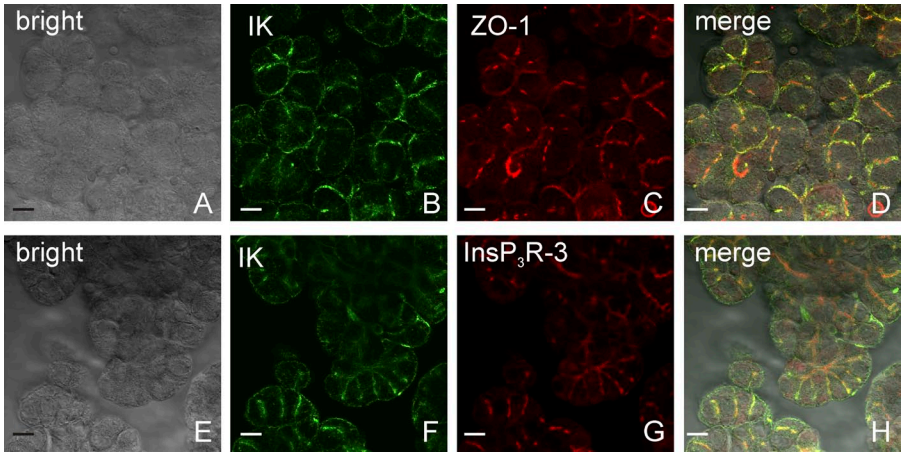

Figure 7. Localization of IK in parotid clumps by immunofluorescence. Immunofluorescence experiments were performed as described in Materials and methods. (A and E) Transmitted laser light images of the parotid clusters. (B and F) The localization of IK is shown and illustrates a prominent PM distribution with enriched localization of channels to the apical domain of the cells. (C) The distribution of the tight junction marker ZO-1 in the clump of cells stained with IK antibodies in B. (G) The localization of $InsP_3R$-3, known to localize to the ER juxtaposed to the apical PM, is shown in the same cells. (D) The overlap of IK and ZO-1 is shown. (H) The co-distribution of IK and $InsP_3R$-3. Bar, 10 µm. Each image is a single z slice acquired at an approximately equatorial plane.

In the mathematical model of Palk et al. (2010), the rate of fluid secretion was optimum if 100% of the Cl^- and between 20 and 40% of the whole cell K^+ conductance was localized specifically to the apical PM. This localization was predicted to efficiently maintain the driving force for Cl^- exit locally at the apical PM by effectively eliminating the contribution of the electrical resistance of the tight junctions. In contrast, as the percentage of K^+ conductance in the apical PM was further increased, the flow rate was predicted to decrease, and ultimately, when K channels were exclusively localized apically, secretion was effectively arrested. Although our data indicate that the K channel density is relatively higher in the apical PM than in basolateral regions, the current experiments do not provide any information regarding the absolute numbers of channels in each domain but are clearly consistent with a fraction, but not exclusive, distribution of K channels to the apical PM.

The apical domain of exocrine cells is specialized structurally and functionally such that the Ca^{2+}-signaling machinery and the important downstream effectors of the Ca^{2+} signal are closely localized (Kiselyov et al., 2006). The localization is proposed to facilitate close coupling between the Ca^{2+} signals and the Cl channels in the apical PM (Giovannucci et al., 2002). In a similar manner, localization of a portion of the complement of K channels would be predicted to ensure rapid activation, essentially simultaneously with Cl channels. This domain has been termed the Ca^{2+} "trigger zone" because Ca^{2+} signals are initiated here as a function of the high density of $InsP_3R$ distributed to a specialized region of ER associated with the apical PM and actin cytoskeleton terminal web (Lee et al., 1997a,b; Yule et al., 1997). $InsP_3R$ localization is reported to depend on both cholesterol-rich domains and interactions with the actin cytoskeleton (Maximov et al., 2003; Fukatsu et al., 2006; Nagata et al., 2007). Notably, depletion of cholesterol is reported to both disrupt Ca^{2+} signals and also alter the functional interaction between BK and IK in acinar cells (Nagata et al., 2007; Romanenko et al., 2009). These observations are consistent with the colocalization of these proteins. Evidence also exists that BK can physically interact with $InsP_3R$ in aortic smooth muscle (Zhao et al., 2010), and thus, the possibility exists that the K channel–$InsP_3R$ interaction in the signaling trigger zone has a structural as well as functional basis in the apical PM of parotid acinar cells.

The authors wish to thank Jill Thompson for proofreading and helpful input throughout this study. The authors would like to thank Julie Zhang for help with the confocal images. The authors would also like to thank Lyndee Knowlton for excellent technical support throughout the study.

This work was supported by National Institutes of Health grants DE014756 and DE019245.

Lawrence G. Palmer served as editor.

Submitted: 12 September 2011
Accepted: 22 December 2011

REFERENCES

Begenisich, T., T. Nakamoto, C.E. Ovitt, K. Nehrke, C. Brugnara, S.L. Alper, and J.E. Melvin. 2004. Physiological roles of the intermediate conductance, Ca2+-activated potassium channel Kcnn4. *J. Biol. Chem.* 279:47681–47687. http://dx.doi.org/10.1074/jbc.M409627200

Cook, D.I., and J.A. Young. 1989. Effect of K+ channels in the apical plasma membrane on epithelial secretion based on secondary active Cl− transport. *J. Membr. Biol.* 110:139–146. http://dx.doi.org/10.1007/BF01869469

Cook, D.I., E.W. Van Lennep, M.L. Roberts, and J.A. Young. 1994. Secretion by the major salivary glands. *In* Physiology of the Gastrointestinal Tract. Third edition. Raven Press, New York. 1061–1117.

Fukatsu, K., H. Bannai, T. Inoue, and K. Mikoshiba. 2006. 4.1N binding regions of inositol 1,4,5-trisphosphate receptor type 1. *Biochem. Biophys. Res. Commun.* 342:573–576. http://dx.doi.org/10.1016/j.bbrc.2006.02.010

Gin, E., E.J. Crampin, D.A. Brown, T.J. Shuttleworth, D.I. Yule, and J. Sneyd. 2007. A mathematical model of fluid secretion from a parotid acinar cell. *J. Theor. Biol.* 248:64–80. http://dx.doi.org/10.1016/j.jtbi.2007.04.021

Giovannucci, D.R., J.I. Bruce, S.V. Straub, J. Arreola, J. Sneyd, T.J. Shuttleworth, and D.I. Yule. 2002. Cytosolic Ca(2+) and Ca(2+)-activated Cl(−) current dynamics: insights from two functionally distinct mouse exocrine cells. *J. Physiol.* 540:469–484. http://dx.doi.org/10.1113/jphysiol.2001.013453

Harmer, A.R., P.M. Smith, and D.V. Gallacher. 2005. Local and global calcium signals and fluid and electrolyte secretion in mouse submandibular acinar cells. *Am. J. Physiol. Gastrointest. Liver Physiol.* 288:G118–G124. http://dx.doi.org/10.1152/ajpgi.00096.2004

Kiselyov, K., X. Wang, D.M. Shin, W. Zang, and S. Muallem. 2006. Calcium signaling complexes in microdomains of polarized secretory cells. *Cell Calcium.* 40:451–459. http://dx.doi.org/10.1016/j.ceca.2006.08.009

Larina, O., and P. Thorn. 2005. Ca2+ dynamics in salivary acinar cells: distinct morphology of the acinar lumen underlies near-synchronous global Ca2+ responses. *J. Cell Sci.* 118:4131–4139. http://dx.doi.org/10.1242/jcs.02533

Lee, M.G., X. Xu, W. Zeng, J. Diaz, R.J. Wojcikiewicz, T.H. Kuo, F. Wuytack, L. Racymaekers, and S. Muallem. 1997a. Polarized expression of Ca2+ channels in pancreatic and salivary gland cells. Correlation with initiation and propagation of [Ca2+]i waves. *J. Biol. Chem.* 272:15765–15770. http://dx.doi.org/10.1074/jbc.272.25.15765

Lee, M.G., X. Xu, W. Zeng, J. Diaz, T.H. Kuo, F. Wuytack, L. Racymaekers, and S. Muallem. 1997b. Polarized expression of Ca2+ pumps in pancreatic and salivary gland cells. Role in initiation and propagation of [Ca2+]i waves. *J. Biol. Chem.* 272:15771–15776. http://dx.doi.org/10.1074/jbc.272.25.15771

Mangos, J.A., and G. Braun. 1966. Excretion of total solute, sodium and potassium in the saliva of the rat parotid gland. *Pflugers Arch. Gesamte Physiol. Menschen Tiere.* 290:184–192. http://dx.doi.org/10.1007/BF00363695

Mangos, J.A., and N.R. McSherry. 1969. Micropuncture study of sodium and potassium excretion in rat parotid saliva: role of aldosterone. *Proc. Soc. Exp. Biol. Med.* 132:797–801.

Mangos, J.A., G. Braun, and K.F. Hamann. 1966. Micropuncture study of sodium and potassium excretion in the rat parotid saliva. *Pflugers Arch. Gesamte Physiol. Menschen Tiere.* 291:99–106. http://dx.doi.org/10.1007/BF00362655

Manzanares, D., C. Gonzalez, P. Ivonnet, R.S. Chen, M. Valencia-Gattas, G.E. Conner, H.P. Larsson, and M. Salathe. 2011. Functional apical large conductance, Ca2+-activated, and voltage-dependent K+ channels are required for maintenance of airway surface liquid volume. *J. Biol. Chem.* 286:19830–19839. http://dx.doi.org/10.1074/jbc.M110.185074

Maruyama, Y., D.V. Gallacher, and O.H. Petersen. 1983. Voltage and Ca2+-activated K+ channel in baso-lateral acinar cell membranes of mammalian salivary glands. *Nature.* 302:827–829. http://dx.doi.org/10.1038/302827a0

Matsuzaki, T., T. Suzuki, H. Koyama, S. Tanaka, and K. Takata. 1999. Aquaporin-5 (AQP5), a water channel protein, in the rat salivary and lacrimal glands: immunolocalization and effect of secretory stimulation. *Cell Tissue Res.* 295:513–521. http://dx.doi.org/10.1007/s004410051257

Maximov, A., T.S. Tang, and I. Bezprozvanny. 2003. Association of the type 1 inositol (1,4,5)-trisphosphate receptor with 4.1N protein in neurons. *Mol. Cell. Neurosci.* 22:271–283. http://dx.doi.org/10.1016/S1044-7431(02)00027-1

Melvin, J.E., D. Yule, T. Shuttleworth, and T. Begenisich. 2005. Regulation of fluid and electrolyte secretion in salivary gland acinar cells. *Annu. Rev. Physiol.* 67:445–469. http://dx.doi.org/10.1146/annurev.physiol.67.041703.084745

Meredith, A.L., K.S. Thorneloe, M.E. Werner, M.T. Nelson, and R.W. Aldrich. 2004. Overactive bladder and incontinence in the absence of the BK large conductance Ca2+-activated K+ channel. *J. Biol. Chem.* 279:36746–36752. http://dx.doi.org/10.1074/jbc.M405621200

Nagata, J., M.T. Guerra, C.A. Shugrue, D.A. Gomes, N. Nagata, and M.H. Nathanson. 2007. Lipid rafts establish calcium waves in hepatocytes. *Gastroenterology.* 133:256–267. http://dx.doi.org/10.1053/j.gastro.2007.03.115

Nakamoto, T., V.G. Romanenko, A. Takahashi, T. Begenisich, and J.E. Melvin. 2008. Apical maxi-K (KCa1.1) channels mediate K+ secretion by the mouse submandibular exocrine gland. *Am. J. Physiol. Cell Physiol.* 294:C810–C819. http://dx.doi.org/10.1152/ajpcell.00511.2007

Nathanson, M.H., M.B. Fallon, P.J. Padfield, and A.R. Maranto. 1994. Localization of the type 3 inositol 1,4,5-trisphosphate receptor in the Ca2+ wave trigger zone of pancreatic acinar cells. *J. Biol. Chem.* 269:4693–4696.

Nauntofte, B. 1992. Regulation of electrolyte and fluid secretion in salivary acinar cells. *Am. J. Physiol.* 263:G823–G837.

Nehrke, K., C.C. Quinn, and T. Begenisich. 2003. Molecular identification of Ca2+-activated K+ channels in parotid acinar cells. *Am. J. Physiol. Cell Physiol.* 284:C535–C546.

Palk, L., J. Sneyd, T.J. Shuttleworth, D.I. Yule, and E.J. Crampin. 2010. A dynamic model of saliva secretion. *J. Theor. Biol.* 266:625–640. http://dx.doi.org/10.1016/j.jtbi.2010.06.027

Palmer, M.L., E.R. Peitzman, P.J. Maniak, G.C. Sieck, Y.S. Prakash, and S.M. O'Grady. 2011. K(Ca)3.1 channels facilitate K+ secretion or Na+ absorption depending on apical or basolateral P2Y receptor stimulation. *J. Physiol.* 589:3483–3494. http://dx.doi.org/10.1113/jphysiol.2011.207548

Park, K., R.M. Case, and P.D. Brown. 2001. Identification and regulation of K+ and Cl− channels in human parotid acinar cells. *Arch. Oral Biol.* 46:801–810. http://dx.doi.org/10.1016/S0003-9969(01)00047-4

Park, M.K., R.B. Lomax, A.V. Tepikin, and O.H. Petersen. 2001. Local uncaging of caged Ca(2+) reveals distribution of Ca(2+)-activated Cl(−) channels in pancreatic acinar cells. *Proc. Natl. Acad. Sci. USA.* 98:10948–10953. http://dx.doi.org/10.1073/pnas.181353798

Poulsen, J.H., and M. Bundgaard. 1994. Quantitative estimation of the area of luminal and basolateral membranes of rat parotid acinar cells: some physiological applications. *Pflugers Arch.* 429:240–244. http://dx.doi.org/10.1007/BF00374318

Putney, J.W., Jr. 1986. Identification of cellular activation mechanisms associated with salivary secretion. *Annu. Rev. Physiol.* 48:75–88. http://dx.doi.org/10.1146/annurev.ph.48.030186.000451

Romanenko, V.G., T. Nakamoto, A. Srivastava, T. Begenisich, and J.E. Melvin. 2007. Regulation of membrane potential and fluid secretion by Ca2+-activated K+ channels in mouse submandibular glands. *J. Physiol.* 581:801–817. http://dx.doi.org/10.1113/jphysiol.2006.127498

Romanenko, V.G., K.S. Roser, J.E. Melvin, and T. Begenisich. 2009. The role of cell cholesterol and the cytoskeleton in the interaction between IK1 and maxi-K channels. *Am. J. Physiol. Cell Physiol.* 296:C878–C888. http://dx.doi.org/10.1152/ajpcell.00438.2008

Romanenko, V.G., M.A. Catalán, D.A. Brown, I. Putzier, H.C. Hartzell, A.D. Marmorstein, M. Gonzalez-Begne, J.R. Rock, B.D. Harfe, and J.E. Melvin. 2010a. Tmem16A encodes the Ca2+-activated Cl− channel in mouse submandibular salivary gland acinar cells. *J. Biol. Chem.* 285:12990–13001. http://dx.doi.org/10.1074/jbc.M109.068544

Romanenko, V.G., J. Thompson, and T. Begenisich. 2010b. Ca2+-activated K channels in parotid acinar cells: The functional basis for the hyperpolarized activation of BK channels. *Channels (Austin).* 4:278–288.

Schroeder, B.C., T. Cheng, Y.N. Jan, and L.Y. Jan. 2008. Expression cloning of TMEM16A as a calcium-activated chloride channel subunit. *Cell.* 134:1019–1029. http://dx.doi.org/10.1016/j.cell.2008.09.003

Silva, P., J. Stoff, M. Field, L. Fine, J.N. Forrest, and F.H. Epstein. 1977. Mechanism of active chloride secretion by shark rectal gland: role of Na-K-ATPase in chloride transport. *Am. J. Physiol.* 233:F298–F306.

Sørensen, J.B., M.S. Nielsen, C.N. Gudme, E.H. Larsen, and R. Nielsen. 2001. Maxi K+ channels co-localised with CFTR in the apical membrane of an exocrine gland acinus: possible involvement in secretion. *Pflugers Arch.* 442:1–11. http://dx.doi.org/10.1007/s004240000493

Strøbaek, D., P. Christophersen, N.R. Holm, P. Moldt, P.K. Ahring, T.E. Johansen, and S.P. Olesen. 1996. Modulation of the Ca(2+)-dependent K+ channel, hslo, by the substituted diphenylurea NS 1608, paxilline and internal Ca2+. *Neuropharmacology.* 35:903–914. http://dx.doi.org/10.1016/0028-3908(96)00096-2

Tan, Y.P., A. Marty, and A. Trautmann. 1992. High density of Ca(2+)-dependent K+ and Cl− channels on the luminal membrane of lacrimal acinar cells. *Proc. Natl. Acad. Sci. USA.* 89:11229–11233. http://dx.doi.org/10.1073/pnas.89.23.11229

Thompson, J., and T. Begenisich. 2006. Membrane-delimited inhibition of maxi-K channel activity by the intermediate conductance Ca^{2+}-activated K channel. *J. Gen. Physiol.* 127:159–169. http://dx.doi.org/10.1085/jgp.200509457

Thompson, J., and T. Begenisich. 2009. Mechanistic details of BK channel inhibition by the intermediate conductance, Ca2+-activated K channel. *Channels (Austin).* 3:194–204.

Turner, R.J., and H. Sugiya. 2002. Understanding salivary fluid and protein secretion. *Oral Dis.* 8:3–11. http://dx.doi.org/10.1034/j.1601-0825.2002.10815.x

Turner, R.J., M. Paulais, M. Manganel, S.I. Lee, A. Moran, and J.E. Melvin. 1993. Ion and water transport mechanisms in salivary glands. *Crit. Rev. Oral Biol. Med.* 4:385–391.

Wegman, E.A., T. Ishikawa, J.A. Young, and D.I. Cook. 1992. Cation channels in basolateral membranes of sheep parotid secretory cells. *Am. J. Physiol.* 263:G786–G794.

Won, J.H., and D.I. Yule. 2006. Measurement of Ca2+ signaling dynamics in exocrine cells with total internal reflection microscopy. *Am. J. Physiol. Gastrointest. Liver Physiol.* 291:G146–G155. http://dx.doi.org/10.1152/ajpgi.00003.2006

Won, J.H., W.J. Cottrell, T.H. Foster, and D.I. Yule. 2007. Ca2+ release dynamics in parotid and pancreatic exocrine acinar cells evoked by spatially limited flash photolysis. *Am. J. Physiol. Gastrointest. Liver Physiol.* 293:G1166–G1177. http://dx.doi.org/10.1152/ajpgi.00352.2007

Wulff, H., M.J. Miller, W. Hansel, S. Grissmer, M.D. Cahalan, and K.G. Chandy. 2000. Design of a potent and selective inhibitor of the intermediate-conductance Ca2+-activated K+ channel, IKCa1: a potential immunosuppressant. *Proc. Natl. Acad. Sci. USA.* 97:8151–8156. http://dx.doi.org/10.1073/pnas.97.14.8151

Yang, Y.D., H. Cho, J.Y. Koo, M.H. Tak, Y. Cho, W.S. Shim, S.P. Park, J. Lee, B. Lee, B.M. Kim, et al. 2008. TMEM16A confers receptor-activated calcium-dependent chloride conductance. *Nature.* 455:1210–1215. http://dx.doi.org/10.1038/nature07313

Young, J.A., and E. Schögel. 1966. Micropuncture investigation of sodium and potassium excretion in rat submaxillary saliva. *Pflugers Arch. Gesamte Physiol. Menschen Tiere.* 291:85–98. http://dx.doi.org/10.1007/BF00362654

Yule, D.I., S.A. Ernst, H. Ohnishi, and R.J. Wojcikiewicz. 1997. Evidence that zymogen granules are not a physiologically relevant calcium pool. Defining the distribution of inositol 1,4,5-trisphosphate receptors in pancreatic acinar cells. *J. Biol. Chem.* 272:9093–9098. http://dx.doi.org/10.1074/jbc.272.14.9093

Zhao, G., Z.P. Neeb, M.D. Leo, J. Pachuau, A. Adebiyi, K. Ouyang, J. Chen, and J.H. Jaggar. 2010. Type 1 IP3 receptors activate BKCa channels via local molecular coupling in arterial smooth muscle cells. *J. Gen. Physiol.* 136:283–291. http://dx.doi.org/10.1085/jgp.201010453